2D Array design based on Fermat Spiral for ultrasound imaging

Oscar Martínez-Graullera[*,a], Carlos J. Martín[a], Gregorio Godoy[b], Luis G. Ullate[a]

[a] *Departamento de Sistemas, Instituto de Automática Industrial-CSIC, Arganda del Rey (Madrid), Spain*
[b] *Departamento de Ingeniería Electrónica de Telecomunicación y Automática, Universidad de Jaén, Linares (Jaén), Spain*

Abstract

The main challenge faced by 3D ultrasonic imaging with 2D array transducers is the large number of elements required to achieve an acceptable level of quality in the images. Therefore, the optimisation of the array layout, in order to reduce the number of active elements in the aperture, has been a research topic in the last years. Nowadays, array technology has made viable the production of 2D arrays with larger flexibility on elements size, shape and position, allowing to study other configurations different to the clasical matrix organization, such as circular, archimedes spiral or polygonal layout between others.

In this work, the problem of designing an imaging system array with large apertures and a very limited number of active elements (N_e =128 and N_e= 256) using the Fermat spiral layout has been studied. As summary, a general discussion about the most interesting cases is presented.

Key words: 2D sparse arrays, 3D ultrasound imaging, Fermat spiral.
PACS: 87.57.-s, 87.63.dh, 43.60.Fg, 43.38.Hz, 43.35.Zc

[*]Corresponding author: Tel.: +34918711900, fax: +34918717050.
e-mail address: oscarm@iai.csic.es

1. Introduction

The development of ultrasonic volumetric imaging is strongly tied to the development of the 2D array transducer. In this way, the main challenge is determined by the large number of elements required to achieve an acceptable level of quality in the images. As in the linear array case, to avoid the formation of grating lobes and, consequently, artifacts in the image, the 2D transducer should have a distance between array elements limited to $\lambda/2$. On the other hand, we need large apertures if a high resolution is desired. Thus, a 60λ diameter aperture, that provides a lateral resolution of 1^o, needs more than 14000 elements to satisfy the $\lambda/2$ condition. These conditions force several problems [1]: (1) the requirement of thousands of elements, which increase the complexity of the transducer manufacture; (2) the small size of the elements, which is associated to low signal-to-noise ratios; (3) the requirement of thousands of electronic channels that increase the cost and complexity of the imaging systems; and (4) the severe fabrication difficulties of the electrical connections.

These problems represent a technological challenge, and around them are organised the main research lines in array design. To overcome this difficulties and reduce the cost and complexity of a 3-D system, undersampling the 2-D array by only connecting some of the elements available is a viable strategy. Then, the aim of array design is to select those elements that produce the most appropriate beampattern or image for a given set of constraints [1].

Traditionally, sparse arrays have been based on the matrix distribution, and several solutions like random distributions [2], Vernier models or optimised distributions have been developed [3, 4]. Other solutions based on curved distribution of the elements, like circular or spiral [5, 6] also have been proposed with better results than the square matrix array, but with a reduced impact in the audience, probably due to their complex manufacture. In the last years, the array technology has made possible the production of 2D arrays with larger flexibility on the elements size, shape and position, providing new options in 2D array design [7].

Looking for a new pattern with reduced periodicity to distribute the elements in the aperture, this work is focused on the Fermat Spiral. Although the spiral layout has been attended in previous studies [5], the Fermat spiral has not been studied yet. Then, our main objective is to evaluate its performance as 2D sparse array. Some considerations have been done to focus the work in a specific problem:

1. The total number of elements in the aperture is limited to 256.
2. Apertures of 40λ, 50λ and 60λ diameter have been designed. Several degrees of reduction have been achieved: 97%, 96% and 94%.
3. The minimum distance between elements is limited to λ, in order to allow increase the element area up to this size.
4. The desired dynamic range in wideband should be more than -45dB, in order to be a usable aperture for Non Destructive Testing applications.

2. Fermat spiral distribution

Fermat spiral is defined by the divergence angle α that determines the angular distance between two consecutive elements. The radial position of each element is determined by the square root of its angular position.

$$x_n = (R_n, \alpha_i) = \left(R_0\sqrt{n\alpha}, n\alpha\right), n = 0, ...(N_e - 1) \tag{1}$$

where the element centre x_n is defined by its polar coordinates and N_e is the number of elements. R_0 is a constant value to achieve the desired aperture size, and it is defined as:

$$R_0 = \frac{D}{2\sqrt{(N_e - 1)\alpha}} \tag{2}$$

where D is the aperture diameter.

In Figure 1 different spiral arrangements with different number of elements (N_e=128, 256) and divergence angles (α= 9^o, 174^o, 116^o, 92^o, 137.51^o) are presented. It can be seen that, although the divergence angle draws just one line, each spiral seems to be configured with a different number of branches, or

inner spirals, which grow from the centre of the array and change its pattern with the inclusion of more elements. We have named the configurations of Figure 1 as SPx, where x is the number of identified branches.

A special case happens when α= 137.51, presented at the bottom of Figure 1 as Golden Angle. This is a well-known angle because it is able to construct a sunflower pattern that has been object of attention in several research areas. This spiral exhibits 34 clockwise spirals and 21 counterclockwise spirals, and it is considered an optimum configuration of seed packaging due to the interelement distance is almost constant [8, 9].

In our opinion, there are several points that make this spiral interesting for array design.

1. Only the divergence angle and the number of elements are needed to define the layout.
2. It is a biological pattern, which in fact it is used by Phyllotaxis as a reference to model several leaves arrangements.
3. The outer elements show a more compact distribution than other spiral layouts, like Archimedean, Hyperbolic, Lituus or Logarithmic. This compactness leads to the element shadowing effect described in [5] and [6].
4. Although elements are organised following a determined line, they compose other spiral structures in the layout. This particular arrangement distributes the contribution of the elements in the grating lobes, which are extended over wide but well located areas, reducing its general level.

In this work, assuming that the number of elements in the aperture is limited to 256 and the minimum distance between them is λ, we propose two kinds of configurations with different design strategies to be analysed:

- The Fermat (128,128) Configuration, F(128,128): The global array is composed by two spirals of 128 elements each ($N_e = 128$), one for emission and other for reception. A design strategy based on the multiplicative nature of the pulse-echo process has been applied to combine both apertures in order to reduce the general grating lobe level in the image system.

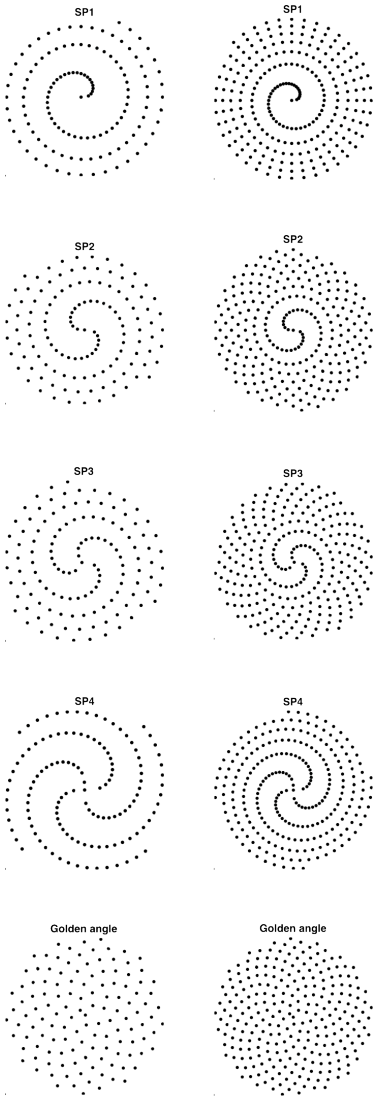

Figure 1: In every row there are different spiral arrangements for different divergence angles (α= 9^o, 174^o, 116^o, 92^o, 137.51^o) and different number of elements (N_e = 128 and 256). We have classified them in SP1, SP2, SP3 and SP4, according to the formation of branches. Divergence angle α=137.51^o corresponds to the sunflower pattern and it is known as Golden Angle

- The Fermat 256 Configuration, F(256): The global array is composed by one spiral of 256 elements ($N_e = 256$), being used the same aperture for emission and reception.

The best cases for the 60λ, 50λ and 40λ diameter apertures in wide-band have been identified, and their performances have been evaluated. The special case of the sunflower pattern ($\alpha = 137.51^o$) is analysed due to its particular relevance.

With the aim in obtaining the best apertures, an exhaustive search based on the divergence angle has been done. Fortunately, the aperture designing conditions reduce the total amount of cases under study. Furthermore, the diameter normalisation $R_{N_e} = R_0$ generates symmetries in the aperture layout that can be used to reduce the total amount of apertures and consequently the set of apertures can be reduced to a viable solutions of α in (0^o: 0.005^o: 180^o).

2.1. Analysis tools

In figure 2 the coordinate system used to evaluate the diffraction response in the hemisphere is presented. For simplicity, the hemisphere is presented as a disk by its projection over the XY plane. Several examples can be seen in figure 3. To evaluate the performance of the possible solutions, two different analytical tools have been used, dividing the analysis in two stages.

In the first one, the analysis has been based on the Array Factor (AF), using an array model of punctual elements, narrowband excitation and far field approximation.

$$|AF(\theta,\phi)| = \left| \sum_{i=1}^{N_e} \exp^{-jk((x_i \cos\phi + y_i \sin\phi)\sin\theta - \xi_i(\theta_o,\phi_o))} \right| \tag{3}$$

where (x_i, y_i) are the cartesian coordinates of the i^{th} element and $\xi_i(\theta_o, \phi_o)$ is the corresponding phase delay value to focus on (θ_o, α_o).

$$\xi_i(\theta_o,\phi_o) = (x_i \cos\phi_o + y_i \sin\phi_o)\sin\theta_o \tag{4}$$

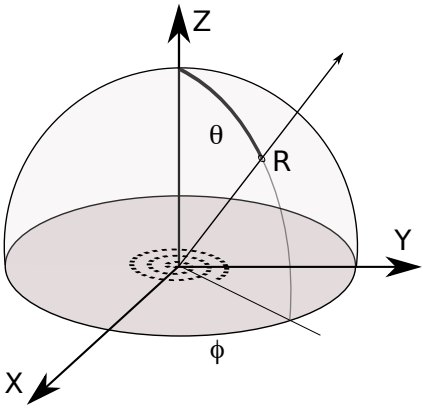

Figure 2: Coordinate system used to compute de array beampattern. The array is located in the XY plane ($\theta = 0$) and the field is computed in a hemisphere, defined for narrowband by (θ, ϕ) and for wideband by (R, θ, ϕ).

The Array Factor allows us to understand how the diffraction pattern is developed with the divergence angle and the number of elements, and help us to design the most appropriated strategy to improve the array performance. Figure 3 shows an example of the Array Factor in the plane ($\theta = 0^o : 30^o, \phi = 0^o : 360^o$) for $\xi_{\theta_o,\phi_o} = 0$, three different divergence angles, and $N_e = 128$ and $N_e = 256$. It can be seen how grating lobes are organized in branches, generating different diffraction patterns for each divergence angle. In spite of the divergence angle is maintained for both values of N_e, except for the golden angle, the beampattern structure changes radically if the number of elements is increased. For this reason it is difficult to transfer the results obtained from one configuration to other, and consequently both configutations have to be analysed independently.

The Array Factor response in pulse-echo can be evaluated using:

$$|AF_{er}(\theta, \phi)| = |AF_e(\theta, \phi) AF_r(\theta, \phi)| \tag{5}$$

where $AF_e(\theta, \phi)$ and $AF_r(\theta, \phi)$ are respectively the array factor on emission and

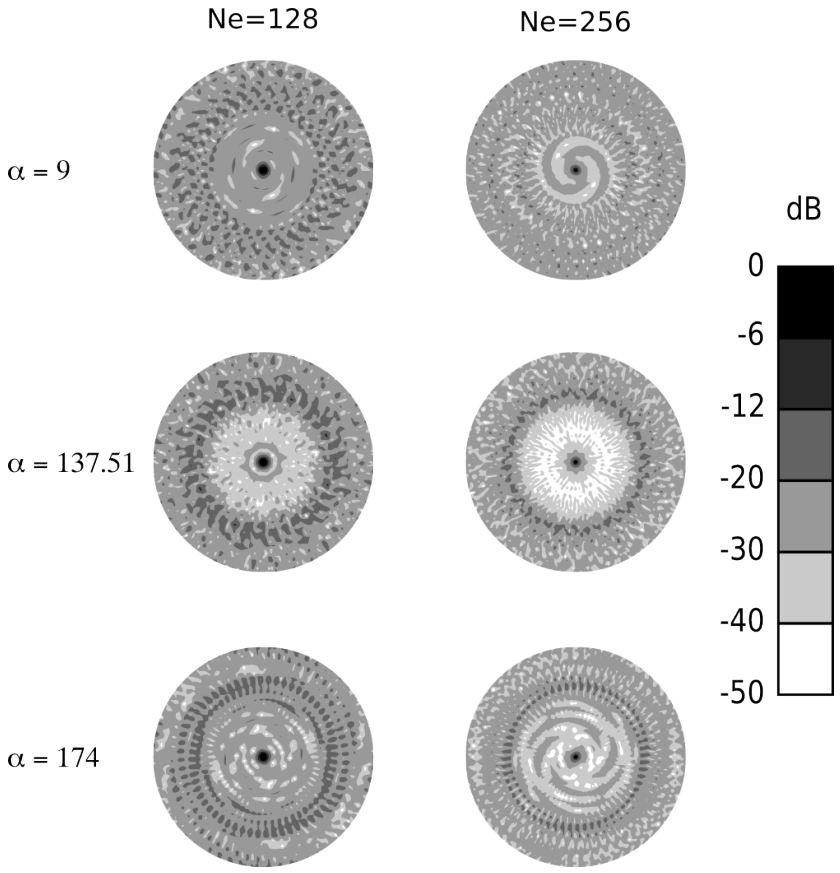

Figure 3: Narrowband Array Factor $\theta = 0^o : 30^o$ for arrangements equals to $\alpha = 9^o$ (SP1), $\alpha = 137.51^o$ and $\alpha = 174^o$ (SP2), and values of $N_e = 128$ and $N_e = 256$

reception of aperture, which are computed by equation 3.

In the second stage, a wideband analysis based on the computation of the acoustic pressure is applied:

$$s(\vec{x},t) = \frac{1}{c^2}\frac{\partial^2 v(t)}{\partial t^2} * \{h_T(\vec{x},t) * h_R(\vec{x},t)\} \tag{6}$$

where $h_T(\vec{x},t)$ and $h_R(\vec{x},t)$ are the emitting and the receiving spatial impulse response of the array, and $v(t)$ is the excitation signal. To reduce the computational cost and suppress the element diffraction response, each one has been reduced to a pointwise located at the center of the element. Then, the spatial impulse response of the array is computed as:

$$h(\vec{x},t) = \sum_{i=1}^{N_e} \frac{\delta(t - \frac{r_i}{c} - T_i)}{2\pi r_i} \tag{7}$$

where r_i is the distance from the center of the i^{th} element to the field point $\vec{x}$, and T_i is the corresponding focussing delay. Then, using the equation 7 to model the emission and the reception arrays in equation 6, the presure wave obtained is determined mainly by the excitation pulse and the element distribution in the aperture.

The Point Spread Function (PSF) in wide-band in a $\vec{x}$ position can be calcualted by the maximum value of the modulus of $s(\vec{x},t)$. In this work, the PSF has been evaluating in a hemisphere as follow:

$$PSF(\theta,\phi) = \max_t \left(\left| s\left((R = \tfrac{D^2}{(4\lambda)}, \theta, \phi), t \right) \right| \right) \tag{8}$$

In the former expression the acoustic field has been computed in a far field hemisphere ($R = \frac{D^2}{(4\lambda)}, \theta = 0^o : 90^o, \phi = 0^o : 360^o$), focusing on ($R = \frac{D^2}{(4\lambda)}, \theta = 0^o, \phi = 0^o$) in emision and reception.

The following parameters have been considered to evaluating the apertures in wideband: (1) the lateral resolution at two levels of -6dB and -40dB, in order to analyse the sharpness of the main lobe; (2) the grating lobe maximum level, which has been determined analysing the PSF for different signal bandwidths:

60%, 70% and 80%; (3) and finally, the mainlobe-to-sidelobe energy ratio (MSR) as a measurement of how the energy is spread in the field [10].

$$MSR = 20\log\frac{\sum\sum|PSF(\theta,\phi)|^2 ML(\theta,\phi)}{\sum\sum|PSF(\theta,\phi)|^2(1-ML(\theta,\phi))} \tag{9}$$

where $ML(\theta,\phi)$ is a logical function that delimites the main lobe region. Here, due to the nature of the results, we have considered that the main lobe is defined by those points whose pressure amplitude is higher than -40dB:

$$ML(\theta,\phi) = \left(20\log\frac{PSF(\theta,\phi)}{PSF(0,0)} > -40dB\right) \tag{10}$$

All these parameters have been computed in a hemisphere (θ=0^o: 1^o: 90^o, ϕ=0^o: 1^o: 360^o).

3. Analysis of the F(128,128) Configuration.

For the F(128,128) configuration a design strategy based on the multiplicative nature of the pulse-echo process is applied. It has been proposed that an imaging system can be composed by two different apertures in emission and reception, where the grating lobes in emission appear at different positions than the grating lobes in reception. Hence, they are partly suppressed in the two-way response[3, 4, 10].

This principle can be applied to Fermat layouts where grating lobes are located in well defined positions. Rather than search different complementary apertures, we use the same aperture for emission and reception and apply a phase displacement $\Delta\alpha$ between them in order to locate emission and reception grating lobes in complementary angular positions.

Then the arrays that compose the F(128,128) configuration can be determined by the equations:

$$x_{En} = (R_n,\alpha_n) = (R_0\sqrt{n\alpha}, n\alpha), n = 0,...127 \tag{11}$$

$$x_{Rn} = (R_n,\alpha_n) = (R_0\sqrt{n\alpha}, n\alpha + \Delta\alpha), n = 0,...127 \tag{12}$$

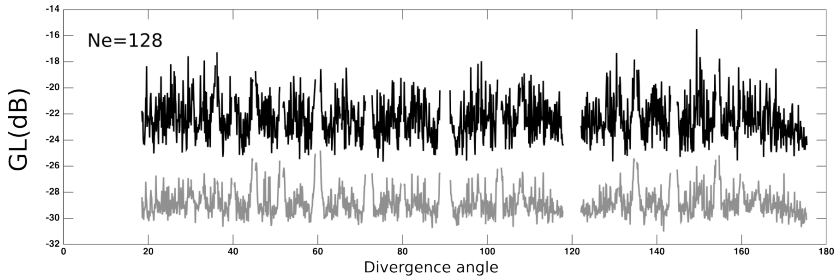

Figure 4: For F(128,128) configuration grating lobe peak (GL) for the narrowband response (two ways) for $\Delta\alpha = 0^o$ (black line) and $\Delta\alpha > 0^o$ (grey line).

where, x_{En} and x_{Rn} are the element centres of the emission and reception apertures.

3.1. Continuos wave analysis

The analysis below is made over 36000 spiral apertures which have been obtained varying the divergence angle. For each one of the viable solutions of spiral apertures for the 60λ diameter aperture, the two way array factor response of all possible complementary apertures ($\Delta\alpha = 0^o : 0.1^o : 180^o$) have been evaluated.

The grating lobe peak values for all the apertures are presented in Figure 4 and summarised in table 1, where the solutions for Golden Angle are also presented. Although the results for the case $\Delta\alpha = 0^o$ are in the range from -15dB to -25.6dB, the combination of two complementary apertures produces a general improvement of the results. The best case arrives then to -31dB.

3.2. Wide band analysis

In spite of the promising results obtained for narrowband signal, its translation to the wideband case (table 1) do not guarantee the achievement of the best results. Our best outcome in narrowband obtains a grating lobe level of -43.6dB in wideband. However, the computation of the wideband (λ=0.5mm,

	Narrow-band		Wide-band	
α	$\Delta\alpha = 0^o$	$\Delta\alpha > 0^o$	$\Delta\alpha = 0^o$	$\Delta\alpha > 0^o$
141.6	-23.7dB	**-31dB**	-40.27dB	-43.61dB
75.4	**-25.6dB**	-30dB	-37.5dB	-39.9dB
137.5	-20.8dB	-27.8dB	-36.2dB	-40.7dB

Table 1: Grating lobe levels for F(128,128) apertures with best results in narrowband ($\Delta\alpha = 0^o$ and $\Delta\alpha > 0^o$); and its corresponding grating lobe levels in wideband. Results for Golden angle are also presented.

BW=60%) grating lobe peak level versus the divergence angle for $\Delta\alpha = 0^o$ produces results of -43dB (figure 5). Then, it is supposed that better results than -43.6dB can be obtained if the search is repeated in wideband.

When $\Delta\alpha = 0^o$ is evaluated for all three apertures it is possible to obtain a general perspective of the grating lobe level distribution to reduce the set of possible solutions. Results are presented in Figure 5. The three aperture diameter present a similar grating lobe distribution however the widest aperture presents more cases, specially for low values of α.

After examining the results, the value of -42.5dB was chosen as a grating lobe threshold to limit the set of apertures to be evaluated in the complementary configuration (figure 5). For D=40λ, 15 cases have been identified with a minimum grating lobe value of -42.78dB. For D=50λ, and D=60λ, 47 and 42 cases have been identified respectively, with a minimum grating lobe value of -43.0dB.

The set of possible solutions is divided in four groups depending of the element organisation (figure 6 and 1).

- SP1: Aperture defined by one branch. Range of divergence angles 8.5^o : 9.5^o. Only available for the widest diameter.

- SP2: Aperture defined by two branches. Range of divergence angles 172.8^o : 175.5^o. This is the one that presents the most number of cases

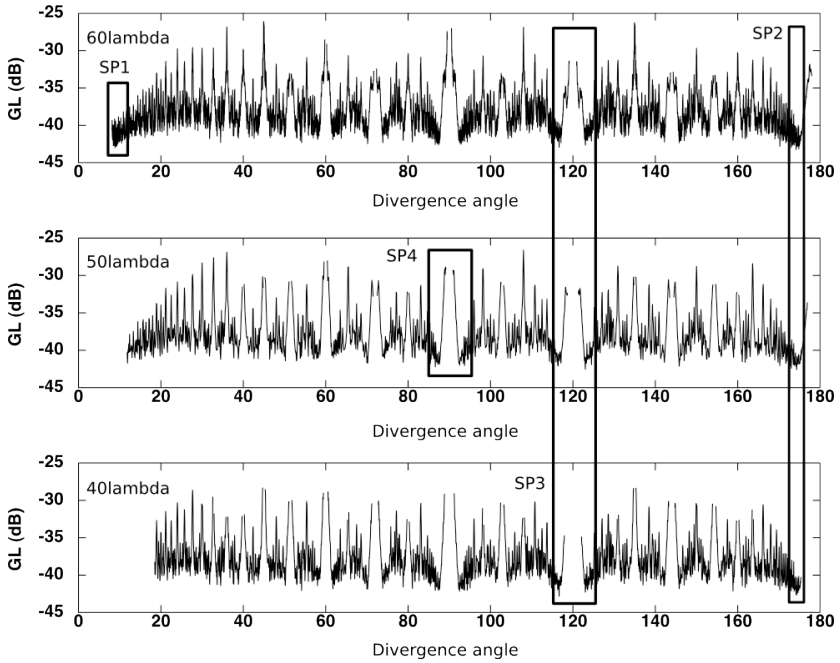

Figure 5: Grating lobe levels vs the divergence angle, for wideband response (two ways, $\Delta\alpha = 0^o$, λ=0.5mm, BW=60%). TOP: Diameter=60λ. MIDDLE: Diameter=50λ. BOTTOM: Diameter=40λ. The locations of the better apertures are indicated by rectangles.

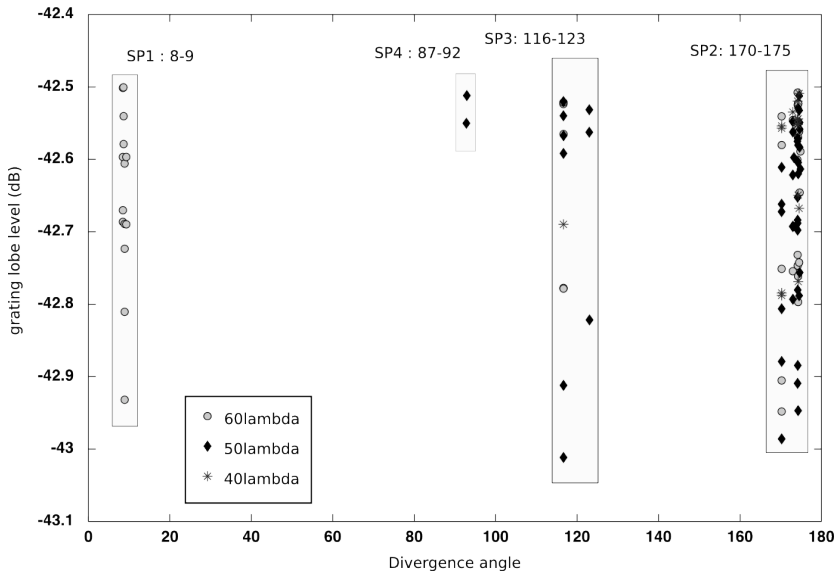

Figure 6: Grating lobe levels vs the divergence angle. Best solutions for $\Delta\alpha = 0^o$ in all the apertures. Circle 60λ, diamond 50λ, asterisk 40λ

and is presented in all the diameter.

- SP3: Aperture defined by three branches. Range of divergence angles $116.5^o : 123.5^o$. It is presented for all the diameter.

- SP4: Aperture defined by four branches. Range of angles $87^o : 93^o$. Only available for D=50λ.

In table 2 the best apertures for each diameter and region are presented. We have also indicated the number of founded cases with a grating lobe peak value lower than -45.5dB (N_a), the lateral resolution, the MSR and the grating lobe for 60%, 70% and 80% signal bandwidth.

In Figure 7, best cases ($\alpha = 174.525^o$ for 40λ and 60λ, and $\alpha = 92.81^o$ for 50λ) and the Golden Angle case ($\alpha = 137.51^o$ for 60λ) beampatterns are presented. In the lateral profiles the maximum, median and minimum grating peak lobe level for each elevation angle are presented. The optimised apertures present almost flat profiles with elevation. Golden Angle configuration presents

Region	N_a	best α	$\Delta\alpha$	D	GL Level (60%) $\Delta\alpha > 0^o$	GL Level (60%) $\Delta\alpha = 0^o$	Lat. Res. -6dB	Lat. Res. -40dB	MSR -40dB	GL level 70%	GL level 80%
SP2	9	174.525^o	46.6^o	40λ	-46.4dB	-42.5dB	1.4^o	4.6^o	18.4dB	-46.5dB	-46.9dB
SP2	30	174.525^o	46.6^o	50λ	-46.3dB	-42.5dB	1.2^o	3.8^o	17.5dB	-46.6dB	-47.0dB
SP3	5	123.045^o	83.7^o	50λ	-46.0dB	-42.8dB	1.2^o	3.8^o	17.4dB	-46.3dB	-46.9dB
SP4	1	92.810^o	46.6^o	50λ	-46.2dB	-42.5dB	1.2^o	4.0^o	17.2dB	-46.5dB	-46.82dB
SP1	7	9.3050^o	66.6^o	60λ	-46.1dB	-42.5dB	1.0^o	3.2^o	17.9dB	-46.1dB	-46.6dB
SP2	18	174.525^o	46.6^o	60λ	-46.4dB	-42.5dB	1.0^o	3.2^o	18.0dB	-46.7dB	-47.0dB
SP3	3	116.64^o	29.82^o	60λ	-45-6dB	-42.5dB	1.0^o	4.8^o	17.8dB	-46.0dB	-46.3dB

Table 2: Performance of the best F(128,128) configurations for each region and diameter. Lateral resolution at -6dB and -40dB and grating lobe level are presented. Grating lobe peak levels for pulse bandwidth of 70% and 80% are also presented.

a high maximum lobes near the main lobe (around 10^o) that is determined by the main distance between elements, which is approximately 5.8λ for the $D = 60\lambda$.

4. Analysis of the F256 Configuration.

As we said in the introduction, we have limited our problem to no more than 256 elements in the aperture. According to our experience in imaging systems design and array manufacturing [11] more than 256 elements in the aperture can be considered a challenge in terms of complexity. Hence, the case of F256 configuration is centred in evaluating the limits of the $N_e = 256$ aperture composed by the same spiral for emission and reception.

The best solution for narrowband (pulse-echo) is for $\alpha = 52.6^o$ with -31.4dB (figure 8). That is 6dB lower than the F(128,128) configuration ($\Delta\alpha = 0$) and equivalent to the best F(128,128) configuration in narrowband ($\Delta\alpha > 0$). For wideband response this solution produces -41.6dB, which is worst than the solution obtained for F(128,128). Therefore a wideband analysis has been done in order to find a better aperture.

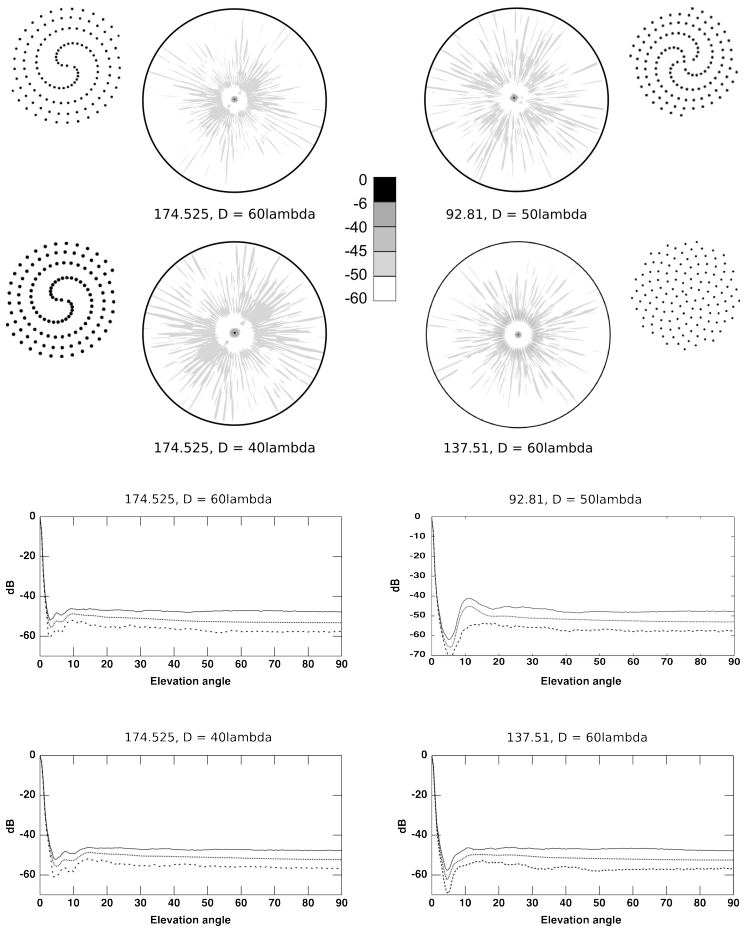

Figure 7: Best cases for F(128,128) $\alpha = 174.525^o$ for 60λ and 40λ; and $\alpha = 92.81^o$ for 50λ configuration and Golden Angle ($\alpha = 137.51^o$ for 60λ) case. Contour profile of the beampattern (top) and in the lateral profiles the maximum, median and minimum grating peak lobe level at each elevation angle are presented (bottom).

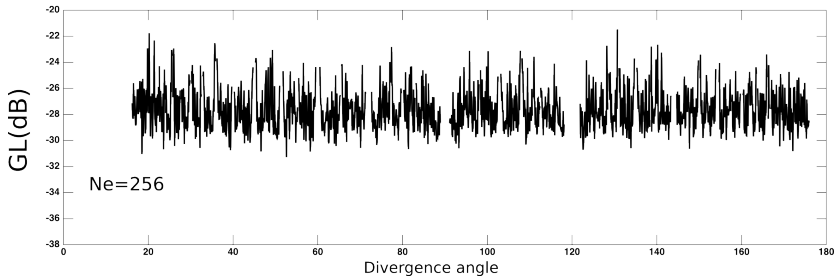

Figure 8: For F(256) configuration grating lobe peak levels for narrowband response (two ways).

All possible solutions of α have been evaluated for diameters of 40λ, 50λ and 60λ and a bandwidth of 60%. These three diameters present a similar grating lobe distribution, improving the results obtained with the F(128,128) configuration. The most interesting cases, those that arrive to -50dB, are presented in table 3. Grating lobe level, lateral resolution and MSR for the selected apertures have been computed. All cases are included in SP4 set.

In figure 9 the best cases and the golden angle case have been presented. The spiral $\alpha = 87.85^o$ has special significance because it is presented in all configurations. Divergence angles 92.05^o and 91.86^o present the same profile but symmetric to the one at angle 87.85^o, confirming that all of them belong to the same family of solutions.

1. Secondary lobes show a particular trace in the region near to the main lobe, which corresponds with the aperture outer profile.
2. In general the secondary lobes are distributed between -50dB and -60dB which means that the distribution is almost flat.

The MSR is around 24dB, being around 7dB higher than the case of F(128,128). The grating lobe level is slightly reduced with an increase of the bandwidth (1dB in the better case). Lateral resolution is maintained around -6dB but it is slightly increased at 40dB with respect to the values obtained in F(128,128).

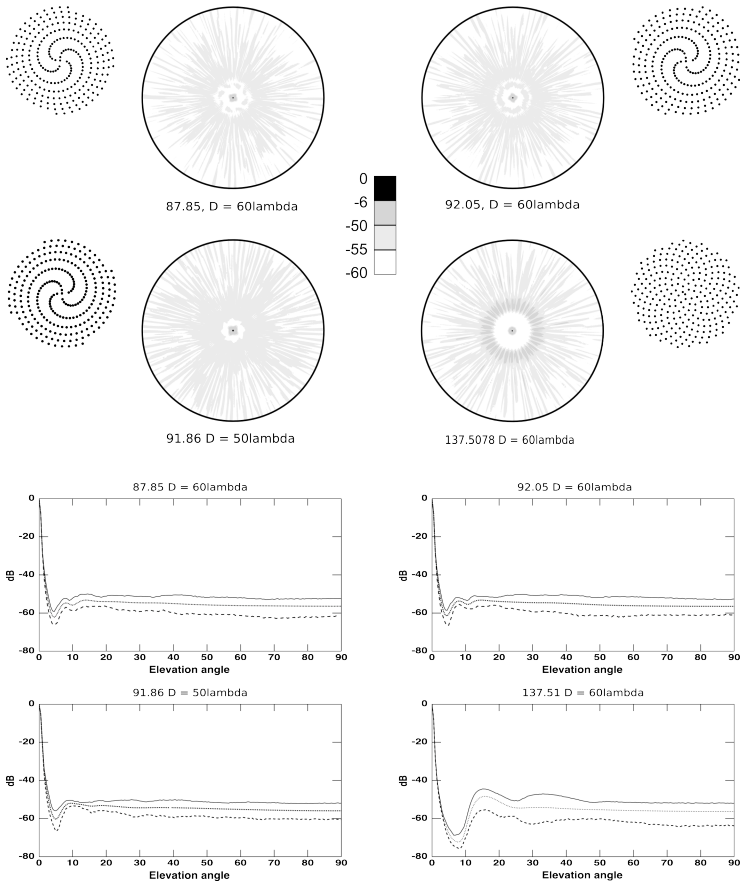

Figure 9: Best cases for F(256) $\alpha = 87.85^o$ and 92.05^o for 60λ and $\alpha = 91.86^o$ for 50λ configuration and Golden Angle ($\alpha = 137.51^o$ for 60λ) case. Contour profile of the beampattern (top) and in the lateral profiles the maximum, median and minimum grating peak lobe level at each elevation angle are presented (bottom).

5. Discussion

In spite of the large amount of cases considered, we can not say that all possible solutions have been obtained. This is due to the high oscillation in the grating lobe level with the divergence angle, and the accuracy needed to its determination. In this sense, the discretization of α and $\Delta\alpha$, imposed to reduce the computational cost, limits our range of solutions.

In spite of this inconvenience, we have identified for both configurations the most representative divergence angles, and proposed apertures that present good performance for imaging applications. However, we can not generalise these results to other configurations easily. As it can be seen in Figure 1 an increase in the number of elements is able to introduce new arrangements in the structure that generates a new grating lobes in the beampattern. Because of this reason the results for the F(256) and F(128,128) configurations are not coincident and are located in different regions: SP4 for F(256) and SP2 for F(128,128) (see in table 2 for $\Delta\alpha = 0^o$).

From the results, we can affirm that the best apertures for each configuration are:

1. $\alpha = 174.525^o$ (SP2) for 128+128, with -46dB of grating lobe peak, which is presented in all the diameters.
2. $\alpha = 87.85^o$ (SP4) for 256, with -50dB of grating lobe peak, which is presented in all the diameters.

The fact that the best solutions for F(256) are located in SP4 can be explained by the increase of the shadowing effect created by the four branches. This has influence in the secondary lobe organisation producing lateral profiles that are almost flat (figure 9), with a reduced margin for optimisation. It is interesting to remark that for F(128,128) and D=50λ it also is possible to find solutions with -46dB in SP4. Probably a more detailed study would reveal solutions for the other diameter apertures.

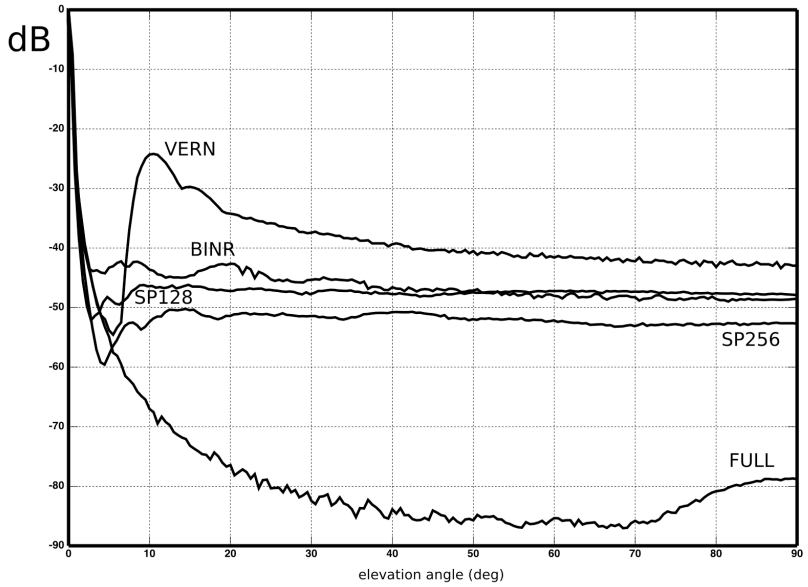

Figure 10: Lateral profiles of the maximum values of pressure in elevation for different sparse apertures and full array.

5.1. Comparative results

To evaluate our results a full array with 120x120 elements (FULL) has been simulated. Furthermore, two disperse apertures next to Ne=128 had been designed for comparison: first, a Vernier (p=9) with (169,169) elements in pulse-echo (VERN) [3]; and second, a bin random array with (121,121) elements in pulse-echo (BINR). It is important to remark that BINR was obtained as the best of 10000 cases evaluated with the Array Factor in a previous work. Figure 10 summarises the results of the comparative study.

The resolution until -20dB is slightly higher for matrix distribution. The spiral apertures present better results for -40dB and -50dB (256 configuration). Grating lobe levels are -42dB and -24dB for BINR and VERN respectively.

5.2. Golden Angle

Divergence Golden Angle produces a set of apertures where the elements are distributed in a compact arrangement such as sunflower pattern, almost equidistance between elements. This kind of distribution produces large grating lobe regions spread around the main beam, in a elevation angle position according to this main distance in the aperture. However, as in the case of annular segmented array, not all the elements contribute simultaneously to each azimuth angle, the magnitude of the grating lobes is reduced with respect to the square matrix distribution. Figures 7 and 9 show the cases for both configurations studied here, where F(128,128) reaches -42.63dB and 256 arrives -44.3dB for the 256.

6. Conclusions

We have shown that the Fermat Spiral is an useful element pattern for sparse array design. The performance of the different spiral configurations is mainly dependent with the number of elements and the divergence angle. We have limited the number of elements in the aperture to 256, so two different configurations have been studied.

- One aperture with 256 elements that operates in emission and reception
- Two different apertures with 128 elements F(128,128), designed with the same divergence angle and combined in order to minimise the grating lobe effect in the image.

Both configurations offer similar results in lateral resolution, which overall is defined by the size of the active aperture. However, the contrast and the dynamic range in the image, which is defined by the grating lobes level and the MSR, produce better results in the F(256) configuration. In fact, the aperture of 256 elements arrives to -50dB which is an adequate dynamic range for most imaging applications.

The F(128,128) configuration produces adequate values for Non Destructive Testing, with a dynamic range of -46dB and good lateral resolution. This

is notable because 128 channels imaging system are available as commercial equipment.

Future works are aimed to evaluate other configurations based on the Fermat Spiral, and to the development of a 128 element array prototype to verify experimentally the efficacy of the proposed distribution.

7. Acknowledgements

This work was supported in part by the Spanish Ministry of Education and Science under grant BES-2005-7704 and the projects DPI2007-65408-C02-01 and TRA2007-67711/AUT.

References

[1] S.W. Smith, H.G. Pavy, O.T. von Ramm, "High-speed ultrasound volumetric imaging system, Part I: Transducer design and beam steering". IEEE Tans. on UFFC. vol 38(2) 1991. pp. 101-108.

[2] W.J Hendricks "Totally random versus the bin approach for random arrays". IEEE Trans on Antennas and Propagation. vol 39(12). 1991. pp. 1757–1761.

[3] G.R. Lockwood, F.S. Foster, "Optimizing the radiation pattern od sparse periodic two-dimensional arrays". IEEE Tans. on UFFC. vol 45(2), 1996, pp. 338–348.

[4] A. Austeng, Sverre Holm. "Sparse 2D arrays for 3D Phased Array Imaging Design Methods". IEEE Tans. on UFFC. vol 49(8), 2002, pp. 1073–1086

[5] J.L. Schwartz and B.D. Steinberg, "Ultrasparse, ultrawideband arrays". IEEE Tans. on UFFC. vol 45(2), 1998, pp. 376-393.

[6] Ullate LG, Godoy G, Martinez O, et al. "Beam steering with segmented annular arrays". IEEE Tans. on UFFC. vol 53 (10), 2006, pp. 1944–1954.

[7] V.Bavaro, G. Caliano, M. Pappalardo. "Element Shape Designo of 2D CMUT Arrays for Reducing Grating Lobes". IEEE Tans. on UFFC. vol 55(2). 2008. pp.308–318.

[8] Roger V. Jean, "Mathematical Modeling in Phyllotaxis: The State of the Art". Mathematical Biosciences. vol 64. 1983. pp. 1–27

[9] J.N. Ridley. "Packing Efficiency in Sunflower Heads". Mathematical Biosciences. vol 58. 1982. pp. 129–139.

[10] S.I. Nikolov, J.A. Jensen "Application of different spatial sampling patterns for sparse array transducer design". Ultrasonics. vol 37. 2000. pp. 667–671

[11] O. Martínez, C.J. Martín, Alberto Octavio, G. Godoy, Francisco Montero de Espinosa, L.G. Ullate, "Increasing the active surface in random sparse 2D arrays". ICU'07. Vienna (Austria). April 2007

		GL (60%)	Lat. Res.		ISPL	GL level	
α	D.	$\Delta\alpha = 0^o$	-6dB	-40dB	-40dB	70%	80%
87.85^o	40λ	-50.0dB	2^o	4.4^o	25.2dB	-50.7dB	-51.1dB
87.85^o	50λ	-50.0dB	1.6^o	3.6^o	24.2dB	-50.9dB	-51.2dB
91.86^o	50λ	-50.0dB	1.6^o	3.4^o	23.6dB	-50.3dB	-50.7dB
87.85^o	60λ	-50.4dB	1.4^o	4.0^o	24.7dB	-50.8dB	-51.2dB
92.05^o	60λ	-50.0dB	1.4^o	3.4^o	24.6dB	-50.4dB	-50.8dB

Table 3: Performance of the best F(256) configurations for each region and diameter. Lateral resolution at -6dB and -40dB and grating lobe level are presented. Grating lobe peak levels for pulse bandwidth of 70% and 80% are also presented.